International Journal of Mass Spectrometry 290 (2010) 113–119

Contents lists available at ScienceDirect

International Journal of Mass Spectrometry

journal homepage: www.elsevier.com/locate/ijms

Theoretical studies on structures and electronic spectra of linear $HC_{2n+1}H^+$ (n = 2–7)

Jinglai Zhang[a,1], Xugeng Guo[a,1], Zexing Cao[b,*]

[a] Institute of Fine Chemistry and Engineering, College of Chemistry and Chemical Engineering, Henan University, Kaifeng 475004, China
[b] Department of Chemistry, State Key Laboratory for Physical Chemistry of Solid Surfaces, Center for Theoretical Chemistry, Xiamen University, Xiamen, Fujian 361005, China

ARTICLE INFO

Article history:
Received 5 November 2009
Accepted 18 December 2009
Available online 29 December 2009

Keywords:
Linear hydrocarbon cations
$HC_{2n+1}H^+$ (n = 2–7)
Theoretical studies
Electronic spectra
Linear size dependence

ABSTRACT

In this work, the odd-numbered linear hydrocarbon cations $HC_{2n+1}H^+$ (n = 2–7) have been investigated with the B3LYP, CAM-B3LYP, and RCCSD(T) calculations focusing on the ground-state geometries, as well as with the CASSCF calculation for the structural optimizations of the ground and first excited states. The present studies reveal that these cation radicals possess stable structures with the ground state of $X^2\Pi_u$ when n is even or $X^2\Pi_g$ when n is odd, featuring some sort of cumulenic character for the middle carbon chains. Consistent with the previous studies of HC_nSi^+ clusters, the odd-numbered HC_nH^+ chains are less stable than the even-numbered ones. The vertical excitation energies for the dipole-allowed $1^2\Pi_{g/u} \leftarrow X^2\Pi_{u/g}$ transitions of $HC_{2n+1}H^+$ (n = 2–7), obtained by the CASPT2/cc-pVTZ level, are 2.59, 2.11, 1.87, 1.65, 1.49, and 1.35 eV, respectively, which mutually agree with the available experimental data of 2.48, 2.07, 1.78, 1.57, 1.42, and 1.29 eV. Particularly the corresponding absorption wavelengths are predicted to have the remarkably linear size dependence, as experimentally observed. In addition, the higher excited electronic transitions of $HC_{2n+1}H^+$ (n = 2–7) are also calculated, indicating that the absorption wavelengths for the $3^2\Pi_{g/u} \leftarrow X^2\Pi_{u/g}$ transitions also exhibit similar linear relationship and the largest oscillator strengths make them accessible more easily in the further experiments.

1. Introduction

In the past decades, polyynes and their derivatives have generated considerable astrophysical and chemical interest owing to their relevance to the interstellar environments [1–4] and chemical processes [5]. It has been suggested that the number of the cyanopolyynes, which have been detected in the space, amounts to 8 [6–13]. In addition, the linear cationic chains HC_nH^+ (n = 4–16) have also been extensively studied, both experimentally and theoretically, leading to reliable reference data about bond lengths, rotational constants, and absorption spectra for these species [14–32].

The polyyne cations $HC_{2n}H^+$, as representative for the open-shell carbon chain radicals, continue to be of special concerns [14–30]. Experimentally, Freivogel et al. [16] and Dzhonson et al. [24] measured the absorption spectra assigned as the $A^2\Pi_{u/g} \leftarrow X^2\Pi_{g/u}$ transitions of $HC_{2n}H^+$ (n = 2–8) in 5 K neon matrices and in the gas phase, respectively. Fulara et al. [25] currently recorded the higher excited electronic transitions of $HC_{2n}H^+$ (n = 2–7) in 6 K neon matrices. Theoretically, Sobolewski and Adamowicz [27] predicted the vertical excitation energies for the $A^2\Pi_{u/g} \leftarrow X^2\Pi_{g/u}$ transitions in $HC_{2n}H^+$ (n = 2–4) with the complete active space second-order perturbation theory (CASPT2). A few years later, Cao and Peyerimhoff [28] calculated the vertical transition energies from the ground to low-lying doublet excited states of HC_6H^+ by means of the multireference configuration interaction (MRCI) method. Recently, Komiha et al. [29] computed the excitation energies of the quartet states in HC_4H^+ and HC_6H^+ using the restricted coupled cluster with perturbative triples [RCCSD(T)] approach.

In contrast to $HC_{2n}H^+$, however, the $HC_{2n+1}H^+$ clusters have attracted little attention [16,17,31,32]. The related studies have only been limited to the absorption spectra of the origin bands for $HC_{2n+1}H^+$ (n = 2–7) in 5 K neon matrices [16,17], as well as the vertical transition energies from the ground to the low-lying excited electronic states of $HC_{2n+1}H^+$ (n = 2–4) by virtue of the *ab initio* MRCI method [31,32]. Accordingly, a better knowledge of ground- and excited-states properties is highly desirable for a better understanding of these species, especially the larger carbon chains. In our previous work, we reported the CASPT2 investigations on the electronic spectra of $HC_{2n}H^+$ (n = 2–8) and found the excellent agreement between the experiments and theoretical calculations [30]. Here, we extend our studies to the $HC_{2n+1}H^+$ (n = 2–7) system at the same theoretical level. The geometric features, atomic charge populations, vibrational frequencies, rotational constants, relative stabilities, and electronic spectra of these linear species are demonstrated. A comparison of the structures and electronic

* Corresponding author. Tel.: +86 592 2186081; fax: +86 592 2183047.
E-mail address: zxcao@xmu.edu.cn (Z. Cao).
[1] Both authors contributed equally to this work.

1387-3806/$ – see front matter © 2009 Elsevier B.V. All rights reserved.
doi:10.1016/j.ijms.2009.12.013

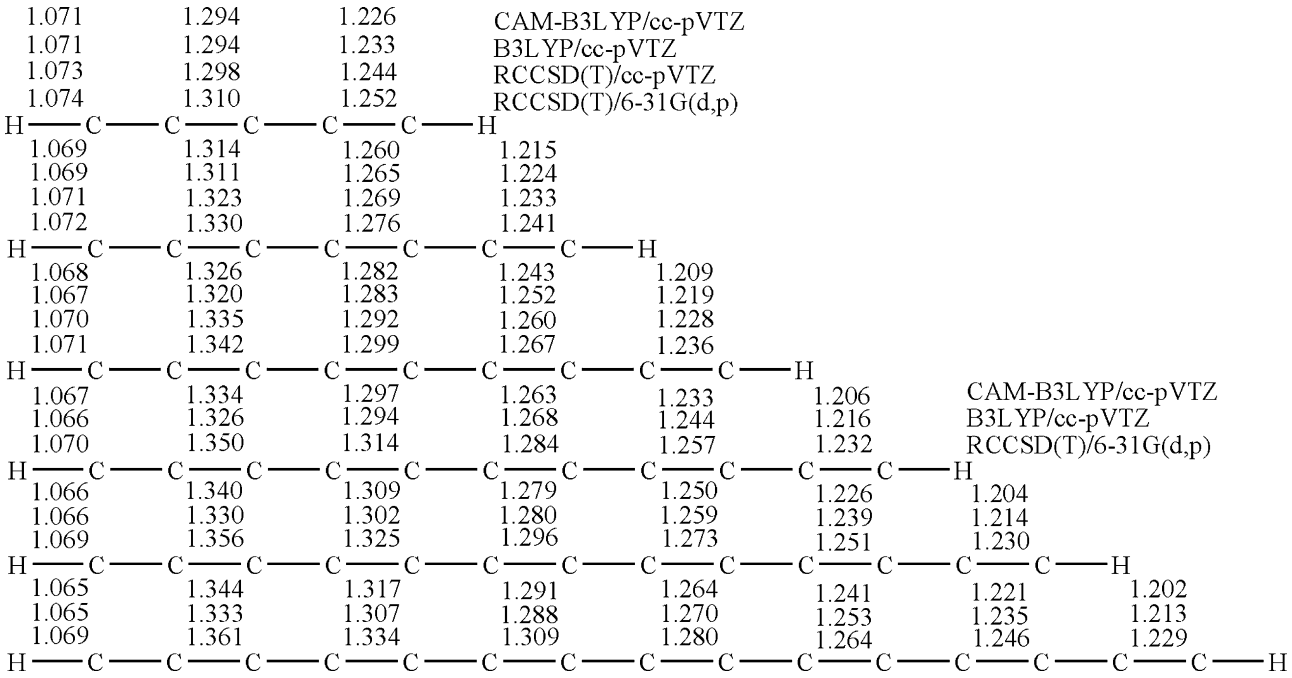

Fig. 1. B3LYP, CAM-B3LYP, and RCCSD(T) optimized bond lengths (in angstrom) of $HC_{2n+1}H^+$ (n = 2–7) cations.

spectra with the $HC_{2n}H^+$ clusters and experimental studies is also presented.

2. Computational details

All electronic structure calculations in the present work have been performed by the Gaussian 09 [33] and MOLPRO 2006 [34] program packages. The B3LYP [35–37] and CAM-B3LYP [38] density functionals with the cc-pVTZ basis set, as well as the RCCSD(T) [39] method with the 6-31G(d,p) basis set, have been used to the full geometry optimizations of their ground states for the linear carbon chain cations $HC_{2n+1}H^+$ (n = 2–7). The RCCSD(T)/cc-pVTZ optimized results for the smaller chains n = 2–4 are also given for a direct comparison. The nature of the optimized structures could be evaluated through the vibrational calculations. In addition, the CASSCF [40,41] approach along with the same 6-31G(d,p) basis set has also been used to optimize the $X^2\Pi_{u/g}$ ground state and the $1^2\Pi_{g/u}$ excited state.

The CASPT2 [42] level of theory with the cc-pVTZ basis set have been used to calculate the vertical excitation energies (ΔE) of the dipole-allowed $(1, 2, 3)^2\Pi_{g/u} \leftarrow X^2\Pi_{u/g}$ transitions and dipole-forbidden $1^2\Phi_{g/u} \leftarrow X^2\Pi_{u/g}$ transitions for $HC_{2n+1}H^+$ (n = 2–7) clusters at the RCCSD(T)/6-31G(d,p) equilibrium geometries. In the CASPT2 calculation, the CASSCF active space is generally composed of the low-energy π valence orbitals, all of which are listed in Table 1, where the first set of eight numbers denote the numbers of inactive (doubly occupied in each configuration) orbitals with symmetry labels A_g, B_{3u}, B_{2u}, B_{1g}, B_{1u}, B_{2g}, B_{3g}, and A_u, respectively, while the last eight numbers are the similar symmetry distribution numbers for the active orbitals.

Generally, the oscillator strengths (f) in the CASPT2 calculations are computed by the formula:

$$f = \frac{2}{3}\Delta E|\mathrm{TM}|^2 \quad (1)$$

where ΔE is the transition energy between the ground and excited states in atomic unit and TM is the transition moment in atomic unit [43].

Table 1
The CASSCF active spaces of $HC_{2n+1}H^+$ (n = 2–7) at the CASPT2 calculations.

Species	CASSCF active space	Electrons
HC_5H^+	(6,0,0,0,5,0,0,0/0,2,2,0,0,2,2,0)	9
HC_7H^+	(8,0,0,0,7,0,0,0/0,3,3,0,0,3,3,0)	13
HC_9H^+	(10,0,0,0,9,0,0,0/0,3,3,0,0,3,3,0)	17
$HC_{11}H^+$	(12,1,1,0,11,0,0,0/0,4,4,0,0,3,3,0)	17
$HC_{13}H^+$	(14,1,1,0,13,1,1,0/0,4,4,0,0,4,4,0)	17
$HC_{15}H^+$	(16,2,2,0,15,1,1,0/0,5,5,0,0,4,4,0)	17

3. Results and discussion

3.1. Optimized ground-state geometries, Mulliken charge populations, vibrational frequencies, rotational constants, and energy differences

3.1.1. Ground-state geometries

Fig. 1 shows B3LYP, CAM-B3LYP, and RCCSD(T) optimized geometries in their ground states of the linear $HC_{2n+1}H^+$ (n = 2–7).

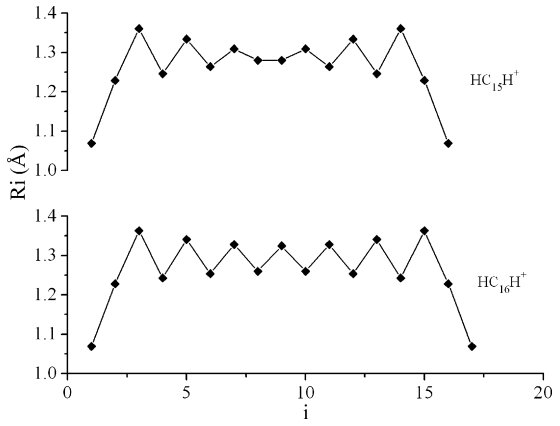

Fig. 2. Bond lengths (in angstrom) of all the bonds along the linear $HC_{15}H^+$ and $HC_{16}H^+$ [30] chains at the RCCSD(T)/6-31G(d,p) level. "i" is numbered starting from one to the other.

Fig. 3. The longitudinal optical (LO) mode of alternating linear carbon chains.

By comparison to the RCCSD(T) results, both the B3LYP and CAM-B3LYP predict similar bond lengths of the equilibrium geometries; however, the bond length alternation (BLA) values by B3LYP are significantly smaller than those by CAM-B3LYP, in accordance with the previous studies on $HC_{2n}H^+$ (n = 2–8) [30] and polyyne oligomers [44]. The RCCSD(T)-predicted bond distances with both basis sets are almost the same and the maximum discrepancy is 0.012 Å from the central C–C bonds in HC_5H^+. It can be therefore concluded that the RCCSD(T)/6-31G(d,p) is a cost-effective level of theory for the structural calculations of these species. At the RCCSD(T)/6-31G(d,p) level, the H–C bond lengths are in the range of 1.069–1.074 Å, bearing essentially the character of single bond, while the adjacent (H)C–C bond lengths are within the 1.229–1.252 Å range, showing a dominant character of triple bond.

For a more thorough comparison of the BLA, as reported in the work of bare carbon chains C_n [45], the geometries of $HC_{15}H^+$ and $HC_{16}H^+$ [30] determined by the same RCCSD(T)/6-31G(d,p) level are depicted in Fig. 2 as a representative example for the odd- or even-numbered carbon chain, respectively. Interestingly, we find that the curve of $HC_{16}H^+$ with the acetylenic structure displays the short/long alternating pattern along the pure carbon chain. For $HC_{15}H^+$, however, the short/long alternation of C–C bond lengths fades out gradually from the two ends to the middle of the chain, exhibiting a character of partial cumulenic structure. Presumably, the notable difference in electronic structure between the odd- and even-numbered linear hydrocarbon cations may lead to the distinct properties of their low-lying excited states to a certain extent.

3.1.2. Mulliken charge populations

The predicted Mulliken atomic charge populations and spin densities of $HC_{2n+1}H^+$ (n = 2–7) are summarized in Table 2. As can be noted in Table 2, the positive charge apparently transfers from the centre to both sides of the chain with increasing number of carbon atoms, which is consistent with those in $HC_{2n}H^+$ (n = 2–8) [30]. However, the spin populations mainly locate around the central carbon atoms, quite different from the $HC_{2n}H^+$ clusters [30]. Such spin distributions means that there is different spin delocalization between the two series.

Table 2
The calculated atomic charge populations and spin densities of $HC_{2n+1}H^+$ (n = 2–7) at the B3LYP/cc-pVTZ level.

n	Atomic chargers (in plain) and spin densities (in italic) from H to central C atoms
2	0.2087, −0.3883, 0.2842, 0.7909 *−0.0104, 0.4248, −0.1480, 0.4672*
3	0.1984, −0.3946, 0.4477, 0.2293, 0.0383 *−0.0080, 0.3300, −0.1271, 0.3754, −0.1407*
4	0.1893, −0.4106, 0.3913, 0.3876, 0.0225, −0.1603 *−0.0065, 0.2679, −0.1115, 0.3157, −0.1347, 0.3383*
5	0.1834, −0.4200, 0.4452, 0.3544, −0.0888, 0.0498, 0.1514 *−0.0055, 0.2243, −0.0968, 0.2699, −0.1257, 0.3032, −0.1387*
6	0.1784, −0.4115, 0.4472, 0.3180, −0.0585, −0.0693, 0.0566, 0.0783 *−0.0047, 0.1919, −0.0850, 0.2345, −0.1146, 0.2720, −0.1372, 0.2863*
7	0.1744, −0.4101, 0.4515, 0.3369, −0.1124, −0.0899, 0.0969, 0.0587, −0.0320 *−0.0041, 0.1666, −0.0754, 0.2063, −0.1043, 0.2450, −0.1306, 0.2670, −0.1412*

Table 3
The selected vibrational frequencies (in cm^{-1}) of $HC_{2n+1}H^+$ (n = 2–7) at the B3LYP/cc-pVTZ level.

Species	Mode	Vibrational frequencies
HC_5H^+	π_u	**127.7**, 405.3, 840.5
	σ_g	783.6, 2053.6, 3379.4
	σ_u	1588.8, 1961.7, 3371.9
HC_7H^+	π_u	**75.9**, 311.0, 808.9
	σ_g	571.8, 1698.4, 2135.0, 3400
	σ_u	1103.1, 1896.1, 2065.4, 3397.0
HC_9H^+	π_u	**47.6**, 222.4, 784.7
	σ_g	450.0, 1275.2, 2063.0, 2154.4, 3413.6
	σ_u	874.4, 1746.8, 1815.0, 2144.3, 3411.8
$HC_{11}H^+$	π_u	**32.8**, 166.7, 767.4
	σ_g	370.8, 1063.1, 1780.1, 2134.8, 2137.3, 3422.8
	σ_u	724.3, 1379.4, 1720.1, 2059.1, 2186.3, 3421.5
$HC_{13}H^+$	π_u	**23.9**, 123.1, 753.7
	σ_g	315.3, 911.7, 1448.7, 2047.7, 2105.8, 2183.9, 3429.2
	σ_u	617.8, 1189.2, 1634.6, 1797.6, 2124.9, 2198.3, 3428.1
$HC_{15}H^+$	π_u	**18.1**, 94.4, 742.9
	σ_g	274.1, 797.6, 1279.0, 1808.1, 2055.5, 2118.3, 2210.6, 3434.1
	σ_u	538.2, 1045.3, 1497.2, 1554.3, 2044.9, 2169.7, 2193.1, 3433.1

The lowest bend frequencies are in bold.

3.1.3. Vibrational frequencies

In order to further understand the nature of the optimized structures we have, in Table 3, collected the harmonic vibrational frequencies of $HC_{2n+1}H^+$ (n = 2–7) chains at the B3LYP equilibrium geometries. We note that the lowest bending frequencies are 127.7, 75.9, 47.6, 32.8, 23.9, and 18.1 cm^{-1}, respectively, all of which are real, suggesting that these cation radicals are stable on the potential energy surface.

In addition, we have also selected, on the basis of the longitudinal optical (LO) mode as shown in Fig. 3, the LO mode frequencies of short linear HC_nH^+ chains (n = 4–16) in Fig. 4, due to the well-known relationship between bond length alternation and the longitudinal C–C stretching modes in linear carbon clusters [46,47]. By symmetry, the LO mode is Raman active for even-numbered n or IR active for odd-numbered n. One can see that the two series of the carbon chains exhibit the similar trend with increasing chain length. However, the frequency of the even-n chains is larger than that of the adjacent odd-n ones, indicating that there is bond strengthening in the structures of for the former, which may make them more stable.

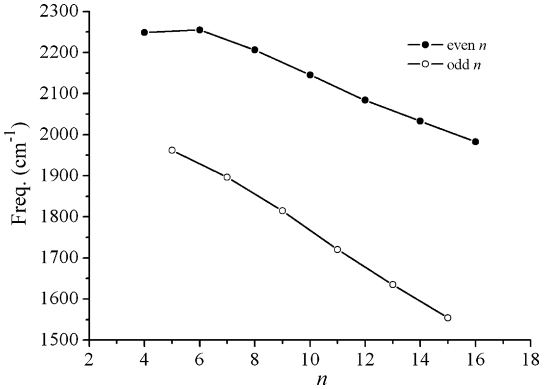

Fig. 4. The longitudinal optical (LO) mode frequencies of the linear carbon clusters HC_nH^+ (n = 4–16) at the B3LYP/cc-pVTZ level.

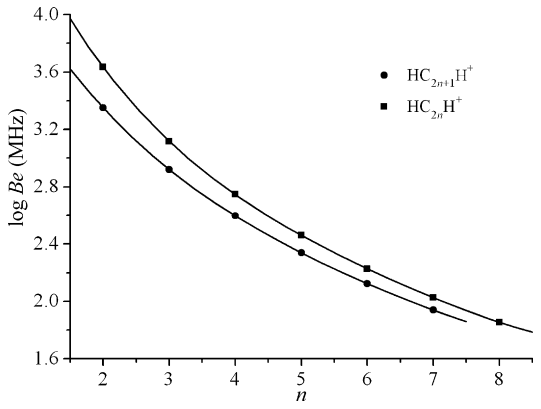

Fig. 5. The calculated rotational constants at the RCCSD(T) optimized geometries of $HC_{2n+1}H^+$ (n = 2–7) cations (below) and $HC_{2n}H^+$ (n = 2–8) cations (above) [30].

3.1.4. Rotational constants

The rotational constants (B_e) of $HC_{2n+1}H^+$ (n = 2–7) obtained using the RCCSD(T)/6-31G(d,p) calculations, as well as the results of $HC_{2n}H^+$ (n = 2–8) [30], are plotted in Fig. 5. As can be seen in Fig. 5, both two curves match very well. For $HC_{2n+1}H^+$, the fitting gives rise to the following equation:

$$\log B_e\ (\mathrm{MHz}) = 5.7572 - 0.9591n + 0.1560n^2 - 0.0153n^3 + 6.25 \times 10^{-4}n^4 \quad (2)$$

where n = 2–7. The fitting error and correlation coefficient are 0.0012 and 1, respectively, revealing high accuracy. As the size of the chain increases, the predicted rotational constant gradually decreases from 2.2413 to 0.0869 GHz on passing from HC_5H^+ to $HC_{15}H^+$.

3.1.5. Energy differences

The energy difference, defined as the difference between the total energies of the adjacent chains, can be used to determine the relative stability of the cationic chains. For the HC_nH^+ chains, the energy difference is calculated as

$$\Delta E_n = E(HC_nH^+) - E(HC_{n-1}H^+) \quad (3)$$

In Fig. 6 is displayed the variation of energy differences (ΔE_n) of the linear HC_nH^+ chains vs. n at the RCCSD(T)/6-31G(d,p) optimized geometries. It can be seen from Fig. 6 that the odd-numbered chains are higher than the even-numbered ones in ΔE_n-values, suggesting that the former are slightly less stable than the latter. This result is accordant with the previous studies on HC_nSi^+ chains [48].

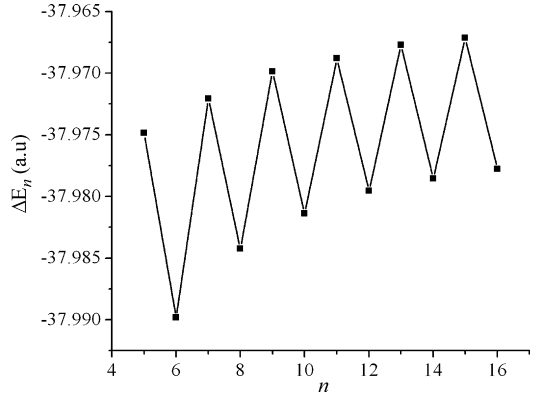

Fig. 6. Energy differences ΔE_n (in atomic unit) of the linear HC_nH^+ (n = 4–16) chains vs. n.

3.2. CASSCF optimized geometries of the $X^2\Pi_{u/g}$ and $1^2\Pi_{g/u}$ states

Depicted in Fig. 7 are the CASSCF optimized geometries of the $X^2\Pi_{u/g}$ ground state and the $1^2\Pi_{g/u}$ excited state for the $HC_{2n+1}H^+$ (n = 2–7) clusters using the CASSCF active spaces in Table 1. It is noticeable that promotion of the electron from $X^2\Pi_{u/g} \rightarrow 1^2\Pi_{g/u}$ leads to the elongation of the shorter C–C bonds (1.190–1.272 Å) and the shortening of the longer C–C bonds (1.276–1.373 Å), compared to the ground state. The relaxation makes the BLA in the excited state less pronounced and the cumulenic feature more remarkable.

3.3. Vertical excitation energies

Table 4 presents the predicted vertical excitation energies (ΔE) and oscillator strengths (f) of the dipole-allowed (1, 2, 3)$^2\Pi_{g/u} \leftarrow X^2\Pi_{u/g}$ transitions as well as the dipole-forbidden $1^2\Phi_{g/u} \leftarrow X^2\Pi_{u/g}$ transitions for the linear $HC_{2n+1}H^+$ (n = 2–7) radicals by the CASPT2 method and the cc-pVTZ basis set. The available experimental data for $HC_{2n+1}H^+$ (n = 2–7) [16,17] and previous MRCI results for $HC_{2n+1}H^+$ (n = 2–4) [31,32] are also given in parentheses.

Among the selected four excited electronic states, the $1^2\Pi_{g/u}$ states are the lowest, derived from the highest occupied molecular orbital (HOMO) to the singly occupied molecular orbital (SOMO), i.e., $n\pi_g \rightarrow (n+1)\pi_u$ for $HC_{4n+1}H^+$ or $(n+1)\pi_u \rightarrow (n+1)\pi_g$ for $HC_{4n+3}H^+$ (n = 1–3). The vertical excitation energies are calculated at 2.59, 2.11, 1.87, 1.65, 1.49, and 1.35 eV, respectively, with the corresponding f-values of 4.58×10^{-4}, 2.23×10^{-4}, 1.18×10^{-3}, 8.98×10^{-4}, 1.94×10^{-3}, and 3.68×10^{-3}, respectively, in very good agreement with the available experimental results of 2.48, 2.07, 1.78, 1.57, 1.42, and 1.29 eV [16,17]. Comparing with the previous MRCI studies on $HC_{2n+1}H^+$ (n = 2–4) [31,32] we find that our estimate for HC_5H^+ is only 0.03 eV higher than the corresponding MRCI value of 2.56 eV [31], whereas our calculations for HC_7H^+ and HC_9H^+ yield much better results than the corresponding MRCI values of 2.34 eV [31] and 2.13 eV [32]. In addition, it is worthy to note that the absorption wavelengths of the origin band for HC_9H^+ reported by the two literatures are not consistent: one is 695 nm [16], and the other is 659 nm [17]. We adopted the former (695 nm) for comparison as it corresponds to the value of the fitting curves in the two literatures.

The next two low-lying excited states are $1^2\Phi_{g/u}$ and $2^2\Pi_{g/u}$, originating from the same electronic excitations as the corresponding $1^2\Pi_{g/u}$ states. The $1^2\Phi_{g/u}$ states are computed at 3.16, 2.59, 2.20, 1.77, 1.66, and 1.47 eV above the ground state, respectively. By the spin and dipole rules, the $1^2\Phi_{g/u} \leftarrow X^2\Pi_{u/g}$ transitions are forbidden. The $2^2\Pi_{g/u}$ states are predicted at 3.49, 2.88, 2.22, 1.95, 1.74, and 1.57 eV, respectively, and the corresponding f-values are 3.42×10^{-2}, 1.19×10^{-2}, 4.90×10^{-4}, 1.91×10^{-3}, 6.29×10^{-4}, and 3.69×10^{-6}, respectively. For the smaller carbon chains, the $2^2\Pi_{g/u} \leftarrow X^2\Pi_{u/g}$ transitions may be found more easily in the further experiments.

The last low-lying $3^2\Pi_{g/u}$ excited states exhibit multireference character, and the two electronic excitations as shown in Table 4 have comparable contribution. The vertical excitation energies locate at 3.57, 2.89, 2.51, 2.18, 1.96, and 1.78 eV, respectively. The largest f-values (6.01×10^{-2}, 1.11×10^{-1}, 1.87×10^{-1}, 1.82×10^{-1}, 2.42×10^{-1}, and 3.25×10^{-1}) make them detectable more easily experimentally.

3.4. Size dependence of absorption wavelengths

As can be found in the experiments, the absorption wavelengths of the origin bands for $HC_{2n+1}H^+$ (n = 2–7) chains have the promi-

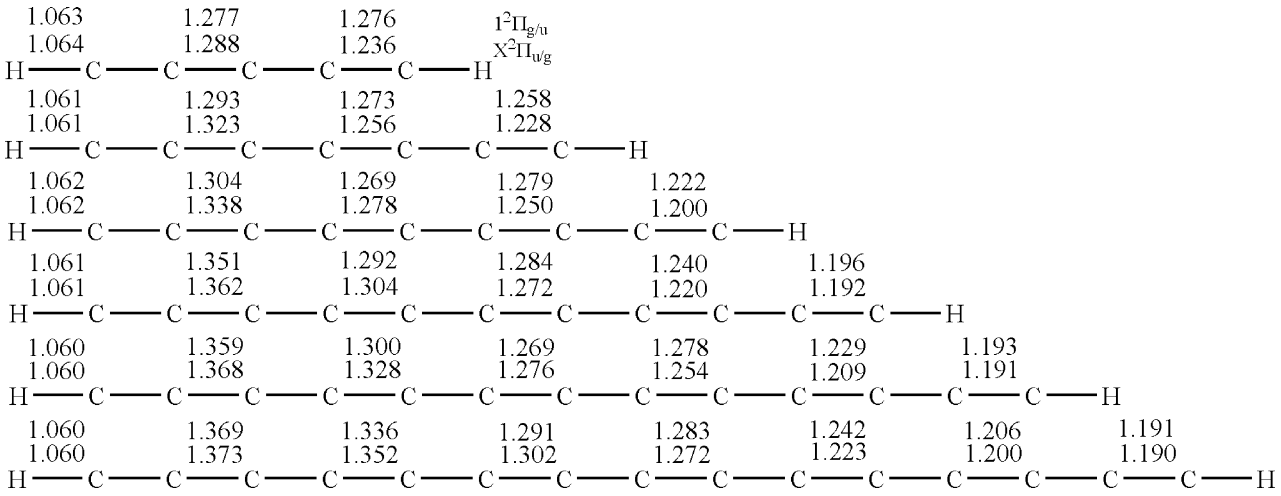

Fig. 7. CASSCF optimized bond lengths (in angstrom) of $HC_{2n+1}H^+$ (n = 2–7) cations.

nently linear size dependence [16,17]. Therefore, a linear fitting for the $1^2\Pi_{g/u} \leftarrow X^2\Pi_{u/g}$ transition energies (λ in nanometer) has been carried out based upon the data in Table 4 (see Fig. 8). The linear fitting curves from the $2^2\Pi_{g/u} \leftarrow X^2\Pi_{u/g}$ and $3^2\Pi_{g/u} \leftarrow X^2\Pi_{u/g}$ transitions are described in Fig. 9 for comparison. These fittings yield the following equation:

$$\lambda = A + Bn \quad (4)$$

where n = 2, 3, ..., 7, and the expression $\lambda[\text{nm}] = 1239.824[\text{nm} \times \text{eV}]/\Delta E[\text{eV}]$ is used.

Table 4
The vertical excitation energies (ΔE, eV) and oscillator strengths (f) of selected four transitions for $HC_{2n+1}H^+$ (n = 2–7) using CASSCF active spaces in Table 1.

Species	State	Excitation		ΔE	f
HC_5H^+	$X^2\Pi_u$	$\cdots 1\pi_u^4 1\pi_g^4 2\pi_u^1 2\pi_g^0$		0.00	
	$1^2\Pi_g$	$1\pi_g \rightarrow 2\pi_u$		2.59 (2.48)[a] (2.56)[b]	4.58×10^{-4}
	$1^2\Phi_g$	$1\pi_g \rightarrow 2\pi_u$		3.16	0.00
	$2^2\Pi_g$	$1\pi_g \rightarrow 2\pi_u$		3.49	3.42×10^{-2}
	$3^2\Pi_g$	$1\pi_g \rightarrow 2\pi_u$	$c^2 = 0.33$	3.57	6.01×10^{-2}
		$(2\pi_u \rightarrow 2\pi_g$	$c^2 = 0.23)$		
HC_7H^+	$X^2\Pi_g$	$\cdots 1\pi_g^4 2\pi_u^4 2\pi_g^1 3\pi_u^0$		0.00	
	$1^2\Pi_u$	$2\pi_u \rightarrow 2\pi_g$		2.11 (2.07)[a] (2.34)[b]	2.23×10^{-4}
	$1^2\Phi_u$	$2\pi_u \rightarrow 2\pi_g$		2.59	0.00
	$2^2\Pi_u$	$2\pi_u \rightarrow 2\pi_g$		2.88	1.19×10^{-2}
	$3^2\Pi_u$	$2\pi_g \rightarrow 3\pi_u$	$c^2 = 0.26$	2.89	1.11×10^{-1}
		$(2\pi_u \rightarrow 2\pi_g$	$c^2 = 0.20)$		
HC_9H^+	$X^2\Pi_u$	$\cdots 2\pi_u^4 2\pi_g^4 3\pi_u^1 3\pi_g^0$		0.00	
	$1^2\Pi_g$	$2\pi_g \rightarrow 3\pi_u$		1.87 (1.78)[a] (2.13)[c]	1.18×10^{-3}
	$1^2\Phi_g$	$2\pi_g \rightarrow 3\pi_u$		2.20	0.00
	$2^2\Pi_g$	$2\pi_g \rightarrow 3\pi_u$		2.22	4.90×10^{-4}
	$3^2\Pi_g$	$3\pi_u \rightarrow 3\pi_g$	$c^2 = 0.39$	2.51	1.87×10^{-1}
		$(2\pi_g \rightarrow 3\pi_u$	$c^2 = 0.18)$		
$HC_{11}H^+$	$X^2\Pi_g$	$\cdots 2\pi_g^4 3\pi_u^4 3\pi_g^1 4\pi_u^0$		0.00	
	$1^2\Pi_u$	$3\pi_u \rightarrow 3\pi_g$		1.65 (1.57)[a]	8.89×10^{-4}
	$1^2\Phi_u$	$3\pi_u \rightarrow 3\pi_g$		1.77	0.00
	$2^2\Pi_u$	$3\pi_u \rightarrow 3\pi_g$		1.95	1.91×10^{-3}
	$3^2\Pi_u$	$3\pi_g \rightarrow 4\pi_u$	$c^2 = 0.40$	2.18	1.82×10^{-1}
		$(3\pi_u \rightarrow 3\pi_g$	$c^2 = 0.18)$		
$HC_{13}H^+$	$X^2\Pi_u$	$\cdots 3\pi_u^4 3\pi_g^4 4\pi_u^1 4\pi_g^0$		0.00	
	$1^2\Pi_g$	$3\pi_g \rightarrow 4\pi_u$		1.49 (1.42)[a]	1.94×10^{-3}
	$1^2\Phi_g$	$3\pi_g \rightarrow 4\pi_u$		1.66	0.00
	$2^2\Pi_g$	$3\pi_g \rightarrow 4\pi_u$		1.74	6.29×10^{-4}
	$3^2\Pi_g$	$4\pi_u \rightarrow 4\pi_g$	$c^2 = 0.41$	1.96	2.42×10^{-1}
		$(3\pi_g \rightarrow 4\pi_u$	$c^2 = 0.17)$		
$HC_{15}H^+$	$X^2\Pi_g$	$\cdots 3\pi_g^4 4\pi_u^4 4\pi_g^1 5\pi_u^0$		0.00	
	$1^2\Pi_u$	$4\pi_u \rightarrow 4\pi_g$		1.35 (1.29)[a]	3.68×10^{-3}
	$1^2\Phi_u$	$4\pi_u \rightarrow 4\pi_g$		1.47	0.00
	$2^2\Pi_u$	$4\pi_u \rightarrow 4\pi_g$		1.57	3.69×10^{-6}
	$3^2\Pi_u$	$4\pi_g \rightarrow 5\pi_u$	$c^2 = 0.41$	1.78	3.25×10^{-1}
		$(4\pi_u \rightarrow 4\pi_g$	$c^2 = 0.17)$		

[a] Experimental values in 5 K neon matrixes from Refs. [16,17].
[b] Previous MRCI values from Ref. [31].
[c] Previous MRCI value from Ref. [32].

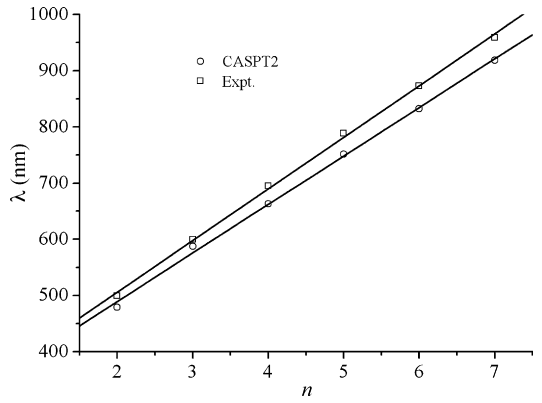

Fig. 8. The linear size dependences of the absorption wavelengths of the $1^2\Pi_{g/u} \leftarrow X^2\Pi_{u/g}$ transitions for $HC_{2n+1}H^+$ (n = 2–7) clusters at the CASPT2 level, as well as the observed values [16,17].

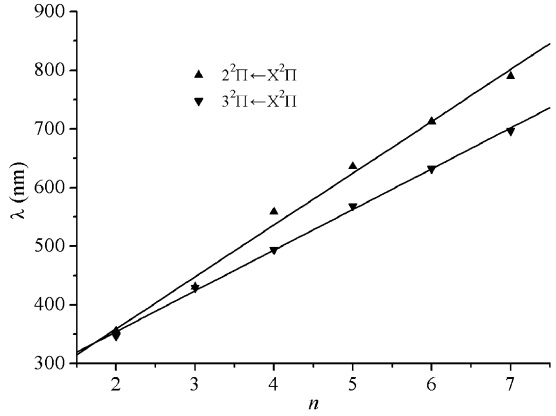

Fig. 9. The linear size dependences of the absorption wavelengths of the $2^2\Pi_{g/u} \leftarrow X^2\Pi_{u/g}$ and $3^2\Pi_{g/u} \leftarrow X^2\Pi_{u/g}$ transitions for $HC_{2n+1}H^+$ (n = 2–7) cations at the CASPT2 level.

For the experimental data, A = 322.46 and B = 91.85. The fitting error and correlation coefficient are 6.42 nm and 0.9994, respectively, exhibiting high accuracy. In the case of the CASPT2 predicted equation, A = 316.86 and B = 86.30, and the fitting error and correlation coefficient are 8.35 nm and 0.9989, respectively. It is apparent that the two curves are very close to each other as displayed in Fig. 8 and the above linear λ–n relationships could reproduce the experimental and calculated data very well. Also, this effect has been observed in the other carbon chains, such as $HC_{2n+1}H$ [17,49] and $HC_{2n}H^+$ [16,17,24,30].

For the $2^2\Pi_{g/u}$ excited states, the fitting error is 16.40 nm, as almost twice as that of the $1^2\Pi_{g/u}$ excited states. Clearly, the linear relationship is less notable as shown in Fig. 9. For the $3^2\Pi_{g/u}$ excited states, however, the fitting error is only 5.91 nm and the linear relationship is quite pronounced.

4. Conclusions

With state of the art theoretical calculations, we reported in this work the equilibrium geometries and electronic spectra of the linear carbon chain radicals $HC_{2n+1}H^+$ (n = 2–7). The present results demonstrate that $HC_{2n+1}H^+$ clusters are observed to have some sort of cumulenic character in the middle of the chains and the BLA in the first excited state is less notable than the corresponding one in the ground state. However, the odd-n cationic chains are difficult to form and more susceptible to fragmentation, due to the lower stabilization than the even-n ones. On the other hand, for the dipole-allowed $1^2\Pi_{g/u} \leftarrow X^2\Pi_{u/g}$ transitions, the agreement between the available experimental results and our theoretical predictions is good, with the largest difference of only 0.11 eV. Furthermore, the corresponding absorption wavelengths exhibit notably linear size dependence, as shown in previous experiments. For the higher transitions, the absorption wavelengths for the $2^2\Pi_{g/u} \leftarrow X^2\Pi_{u/g}$ and $3^2\Pi_{g/u} \leftarrow X^2\Pi_{u/g}$ transitions also show similar linear relationships. Overall, the present calculations provide accurate information for spectroscopists and they should be helpful to the further experimental studies.

Acknowledgements

This project is supported by the National Science Foundation of China (Project Nos.: 20673087, 20733002, and 20873105), the Natural Science Foundation of Henan Province (Nos.: 0311011200 and 200510475012) and the Ministry of Science and Technology (2004CB719902).

References

[1] M.B. Bell, P.A. Feldman, S. Kwok, H.E. Matthews, Nature 295 (1982) 389–391.
[2] J. Fulara, D. Lessen, P. Freivogel, J.P. Maier, Nature 366 (1993) 439–441.
[3] W. Kratschmer, J. Chem. Soc., Faraday Trans. 89 (1993) 2285–2287.
[4] J. Cernicharo, M. Guelin, Astron. Astrophys. 309 (1996) L27–L30.
[5] J.H. Kiefer, S.S. Sidhu, R.D. Kern, K. Xie, H. Chen, L.B. Harding, Combust. Sci. Technol. 82 (1992) 101–130.
[6] M. Guelin, J. Cernicharo, Astron. Astrophys. 244 (1991) L21–L24.
[7] L.M. Ziurys, Proc. Natl. Acad. Sci. U.S.A. 103 (2006) 12274–12279.
[8] A. Fuente, S. Garcia-Burillo, M. Gerin, D. Teyssier, A. Usero, J.R. Rizzo, P. de Vicente, Astrophys. J. 619 (2005) L155–L158.
[9] D. Fosse, J. Cernicharo, M. Gerin, P. Cox, Astrophys. J. 552 (2001) 168–174.
[10] C.M. Walmsley, G. Winnewisser, F. Toelle, Astron. Astrophys. 81 (1980) 245–250.
[11] Q.R. Nguyen, D. Graham, V. Bujarrabal, Astron. Astrophys. 138 (1984) L5–L8.
[12] H.W. Kroto, C. Kirby, D.R.M. Walton, L.W. Avery, N.W. Broten, J.M. MacLeod, T. Oka, Astrophys. J. 219 (1978) L133–L137.
[13] M.B. Bell, P.A. Feldman, M.J. Travers, M.C. McCarthy, C.A. Gottlieb, P. Thaddeus, Astrophys. J. Lett. 483 (1997) L61–L64.
[14] J.H. Callomon, Can. J. Phys. 34 (1956) 1046–1074.
[15] J. Lecoultre, J.P. Maier, M. Rosslein, J. Chem. Phys. 89 (1988) 6081–6085.
[16] P. Freivogel, J. Fulara, D. Lessen, D. Forney, J.P. Maier, Chem. Phys. 189 (1994) 335–341.
[17] J.P. Maier, Chem. Soc. Rev. 26 (1997) 21–28.
[18] D. Klapstein, R. Kuhn, J.P. Maier, M. Ochsner, W. Zambach, J. Phys. Chem. 88 (1984) 5176–5180.
[19] W.E. Sinclair, D. Pfluger, H. Linnartz, J.P. Maier, J. Chem. Phys. 110 (1999) 296–303.
[20] D. Pfluger, W.E. Sinclair, H. Linnartz, J.P. Maier, Chem. Phys. Lett. 313 (1999) 171–178.
[21] R. Raghunandan, F.J. Mazzotti, R. Chauhan, M. Tulej, J.P. Maier, J. Phys. Chem. A 113 (2009) 13402–13407.
[22] D. Pfluger, T. Motylewski, H. Linnartz, W.E. Sinclair, J.P. Maier, Chem. Phys. Lett. 329 (2000) 29–35.
[23] P. Cias, O. Vaizert, A. Denisov, J. Mes, H. Linnartz, J.P. Maier, J. Phys. Chem. A 106 (2002) 9890–9892.
[24] A. Dzhonson, E.B. Jochnowitz, J.P. Maier, J. Phys. Chem. A 111 (2007) 1887–1890.
[25] J. Fulara, M. Grutter, J.P. Maier, J. Phys. Chem. A 111 (2007) 11831–11836.
[26] T. Bally, W. Tang, M. Jungen, Chem. Phys. Lett. 190 (1992) 453–459.
[27] A.L. Sobolewski, L. Adamowicz, J. Chem. Phys. 102 (1995) 394–399.
[28] Z. Cao, S.D. Peyerimhoff, Phys. Chem. Chem. Phys. 3 (2001) 1403–1406.
[29] N. Komiha, P. Rosmus, J.P. Maier, Mol. Phys. 104 (2006) 3281–3285.
[30] J. Zhang, X. Guo, Z. Cao, J. Chem. Phys. 131 (2009) 144307–144313.
[31] M. Mühlhäuser, J. Haubrich, G. Mpourmpakis, A. Mavrandonakis, G.E. Froudakis, Internet Electron. J. Mol. Des. 2 (2003) 578–588.
[32] M. Mühlhäuser, J. Haubrich, S.D. Peyerimhoff, Int. J. Quantum Chem. 100 (2004) 53–58.
[33] M.J. Frisch, G.W. Trucks, H.B. Schlegel, G.E. Scuseria, M.A. Robb, J.R. Cheeseman, G. Scalmani, V. Barone, B. Mennucci, G.A. Petersson, H. Nakatsuji, M. Caricato, X. Li, H.P. Hratchian, A.F. Izmaylov, J. Bloino, G. Zheng, J.L. Sonnenberg, M. Hada, M. Ehara, K. Toyota, R. Fukuda, J. Hasegawa, M. Ishida, T. Nakajima, Y. Honda, O. Kitao, H. Nakai, T. Vreven, J.A. Montgomery Jr., J.E. Peralta, F. Ogliaro, M. Bearpark, J.J. Heyd, E. Brothers, K.N. Kudin, V.N. Staroverov, R. Kobayashi, J. Normand, K. Raghavachari, A. Rendell, J.C. Burant, S.S. Iyengar, J. Tomasi, M. Cossi, N. Rega, J.M. Millam, M. Klene, J.E. Knox, J.B. Cross, V. Bakken, C. Adamo, J. Jaramillo, R. Gomperts, R.E. Stratmann, O. Yazyev, A.J. Austin, R. Cammi, C. Pomelli, J.W. Ochterski, R.L. Martin, K. Morokuma, V.G. Zakrzewski, G.A. Voth, P. Salvador, J.J. Dannenberg, S. Dapprich, A.D. Daniels, O. Farkas, J.B. Foresman, J.V. Ortiz, J. Cioslowski, D.J. Fox, Gaussian 09, Revision A.02, Gaussian, Inc., Wallingford CT, 2009.

[34] MOLPRO 2006.1 is a package of *ab initio* programs written by H.-J. Werner, P.J. Knowles, with contributions from R.D. Amos, A. Bernhardsson, A. Berning, P. Celani, D.L. Cooper, M.J.O. Deegan, A.J. Dobbyn, F. Eckert, C. Hampel, G. Hetzer, T. Korona, R. Lindh, A.W. Lloyd, S.J. McNicholas, F.R. Manby, W. Meyer, M.E. Mura, A. Nicklass, P. Palmieri, R. Pitzer, G. Rauhut, M. Schütz, H. Stoll, A.J. Stone, R. Tarroni, T. Thorsteinsson.
[35] C. Lee, W. Yang, R.G. Parr, Phys. Rev. B37 (1988) 785–789.
[36] B. Miehlich, A. Savin, H. Stoll, H. Preuss, Chem. Phys. Lett. 157 (1989) 200–206.
[37] A.D. Becke, J. Chem. Phys. 98 (1993) 5648–5652.
[38] T. Yanai, D.P. Tew, N.C. Handy, Chem. Phys. Lett. 393 (2004) 51–57.
[39] J.D. Watts, J. Gauss, R.J. Bartlett, J. Chem. Phys. 98 (1993) 8718–8733.
[40] H.-J. Werner, P.J. Knowles, J. Chem. Phys. 82 (1985) 5053–5063.
[41] P.J. Knowles, H.-J. Werner, Chem. Phys. Lett. 115 (1985) 259–267.
[42] P. Celani, H.-J. Werner, J. Chem. Phys. 112 (2000) 5546–5557.
[43] S.D. Peyerimhoff, in: P.von R. Schleyer, N.L. Allinger, T. Clark, J. Gasteiger, P.A. Kollman, H.F. Schaefer, P.R. Schreiner (Eds.), The Encyclopedia of Computational Chemistry, vol. 4, Wiley, Chichester, 1998, p. 2654.
[44] M.J.G. Peach, E.I. Tellgren, P. Salek, T. Helgaker, D.J. Tozer, J. Phys. Chem. A 111 (2007) 11930–11935.
[45] S. Yang, M. Kertesz, J. Phys. Chem. A 112 (2008) 146–151.
[46] J. Kastner, H. Kuzmany, L. Kavan, F.P. Dousek, J. Kürti, Macromolecules 28 (1995) 344–353.
[47] See, e.g.:
(a) N.W. Ashcroft, N.D. Mermin, Solid State Physics, Saunders College, Philadelphia, PA, 1976;
(b) G. Burns, Solid State Physics, Academic, Boston, MA, 1990.
[48] J. Yang, J.Y. Qi, J. Liu, M.D. Chen, Q.E. Zhang, C.T. Au, Int. J. Mass Spectrom. 272 (2008) 172–179.
[49] C. Zhang, Z. Cao, H. Wu, Q. Zhang, Int. J. Quant. Chem. 98 (2004) 299–308.